ROYAL SOCIETY OF CHEMISTRY

PAPER

Quantifying mechanical abrasion of AgNP nanocomposites: influence of AgNP content on abrasion products and rate of microplastic production†

Joana Marie Sipe, [iD] [a] William Berger, [iD] [a] Nathan Bossa,[a] Melissa Chernick, [iD] [b] Keana C. K. Scott, [iD] [c] Alan Kennedy,[d] Mark Ballentine,[d] Treye Thomas,[e] Christine Ogilvie Hendren [iD] [af] and Mark R. Wiesner [iD] *[a]

Nanomaterials are used in polymer composites to enhance plastic products' properties. Silver nanoparticles (AgNPs) are added to composites for their antimicrobial and fungicidal properties. Polyethylene terephthalate glycol polymer (PETG) AgNP composite test objects with AgNP mass fraction of 0.5% and 2% were abraded using NIST SP 1200-30 abrasion protocol to find the microplastic (MP) abrasion rates of these nanocomposites over various power inputs. Results showed that the abrasion rate of composite depended on the polymer matrix rather than on the AgNP content in the product. However, AgNPs affected the size and physico-chemical properties and surface qualities of particles produced. Surface attached and protuberant AgNPs were found on the abraded particles. As the mass fraction of nanomaterial increased in the composite, the size range of abraded composite particles produced during abrasion decreased.

Environmental significance

This paper fits the scope of fate of nanocomposites in the environment and use of nanocomposite release for risk assessment. In this paper, we investigate the abrasion of 3D printed AgNP–PETG composites at three concentrations (0, 0.5, and 2 weight percent) and their fragmentation release rate into microplastics. These particles were then characterized *via* sizing, imaging, and surface characterization. The abrasion rate was then used to create risk-analysis rates for exposure *via* consumer use and environmental breakdown. We conclude that the matrix drives release, however the addition of AgNPs does affect size and surface characterization of microplastics released.

1 Introduction

Increasingly used in many consumer products such as textiles, soaps, and plastics for their anti-bacterial and fungicidal activity,[1,2] AgNPs are perhaps the most widely used metal nanomaterial (NM) in consumer products. With projections of use in antibacterial safety applications estimated to continue on an upward trend, the use of AgNPs appears to have accelerated since the COVID-19 pandemic.[3,4] AgNPs embedded in polymer have been incorporated into fabrics and shown to be released from treated fabric with use.[4,5] AgNPs have also been added to feedstock polymers for objects produced by both 3D printing and cast-molding.[6] In some applications, 3D printing offers clear advantages over cast-molding due to lower processing times and the option of easily customizable shapes and sizes.[7] The use of AgNPs in 3D printed, and other, baby products and the implication of exposure to these NPs have presented some cause for concern.[8,9] In addition, the potential exposure to microplastics (MPs) and nanoplastics produced with the use of these nano-enabled products has generated concerns, as illustrated by recent studies detailing that babies are exposed to much higher levels of polyethylene terephthalate (PET) and polycarbonate (PC) plastics than adults.[10,11]

[a] Department of Civil and Environmental Engineering, Duke University, 120 Hudson Hall, Durham, NC, 27708-0287, USA. E-mail: wiesner@duke.edu

[b] Department of Toxicology, Duke University, Durham, NC, 27708, USA

[c] Materials Measurement Science Division, National Institute of Standards and Technology, 100 Bureau Drive, MS-8372, Gaithersburg, MD 20899, USA

[d] US Army Engineer Research and Development Center, Environmental Laboratory, 3909 Halls Ferry Rd., Vicksburg, MS, USA

[e] United States Consumer Product Safety Commission, 4330 East-West Highway, Bethesda, Maryland 20814, USA

[f] Department of Geological and Environmental Sciences, Appalachian State University, 287 Rivers St., Boone, NC 28608, USA

† Electronic supplementary information (ESI) available. See DOI: https://doi.org/10.1039/d3en00888f

2968 | *Environ. Sci.: Nano*, 2024, **11**, 2968–2977

This journal is © The Royal Society of Chemistry 2024

Quantifying the amounts and kinetics of MPs, nanoplastics, and nanomaterial release from nanocomposites during mechanical abrasion that simulates product use and handling is essential to assessing the risks of these products. This study presents the results of mechanical abrasion study performed on AgNP–PETG (polyethylene terephthalate glycol) composites according to the method discussed in Bossa et al., Sipe et al., and NIST SP-1200-30.[12–14] This method is used to determine the abrasion rate of AgNP composites as a function of power input during mechanical abrasion. From this, input quantities of MPs and nanoplastics for risk assessment and safety modeling can be estimated for different exposure scenarios, e.g., material release during sanding for manufacturers and chewing or mouthing by babies. The abrasion study was performed on PETG and AgNP–PETG nanocomposites with mass fractions of 0.5% and 2% AgNPs. These AgNP mass loadings were chosen to be the same as the nanomaterial mass loadings used in the earlier, accompanying study of MWCNT–PETG nanocomposites for easier comparison.[12] While the AgNP concentrations used in the work are considerably higher than those used in some commercial products, these concentrations were choses to allow for comparison with the effects of other nanofillers on the mechanical properties of the composite and represent a worst-case scenario.

2 Methods

2.1 3D printed polymer preparation

Uncoated AgNPs were obtained from NanoDynamics with reported nominal diameters of 30 nm [ND30].[15] TEM analysis of the AgNPs show that the diameters of the ND30 AgNPs ranged from 20 nm to 50 nm. Fig. 1 shows TEM micrographs of typical AgNP agglomerates. Filament grade PETG (polyethylene terephthalate glycol) was purchased from ChasePlastics (SKYGREEN S2008; Lot # 5000356207). PETG and AgNPs were then processed into PETG (with no AgNPs) and Ag–PETG composite filaments with two different nominal mass fractions of AgNPs (0.5%, and 2%) by the US Army Corps of Engineers Research and Development Center,

Environmental Laboratory using a single extruder (Filabot EX2, Barre, VT, USA). Hereafter, the three composites with different loadings of AgNPs are referenced as PETG, 0.5%Ag and 2%Ag. AgNP composite dog bone shaped specimens (ASTM D638, 1 mm thickness) and cylindrical pucks (diameter of 50.8 mm and thickness of 5 mm) were 3D printed from these filaments as described in Bossa et al.[12] The dog bone specimens were used for composite tensile testing and the pucks were used for abrasion experiments. Pictures of the composites and dog bone shape can be seen in Fig. S1.†

2.2 3D polymer characterization

A Test Resources 830 biaxial tensile test machine (Shakopee, MN) was used to measure the mechanical properties of the composites. Uniaxial tensile tests ($N = 3$) were performed at room temperature, according to ASTM D638, to obtain stress–strain curves and Young's modulus, and ultimate tensile strength of the composites were determined from these data. Hydrophobicity was determined by measuring the water contact angle on the surface of the composite with Nanosight Goniometer Biolin Scientific Attension Theta Flex (Västra, Frölunda Sweden) using the sessile drop method with three replicates on two coupons ($N = 6$).

2.3 Abrasion method

The Taber abrader has been used in many abrasion studies to generate wear particles from polymer and polymer composite surfaces. Cryomills are also commonly used to generate microplastic (MP) particles from bulk plastic material.[16] However, Taber abraders do not provide a complete characterization of the power input during the abrasion process and cryomilling does not provide information on the rate of abrasion or power input. Additionally, cryomilling requires the plastic to be frozen during fragmentation, which may alter the resulting MPs, or nanomaterials. In this work, a custom abrasion setup and protocol previously described in Bossa et al., Sipe et al., and Scott et al. were used to generate MPs and calculate
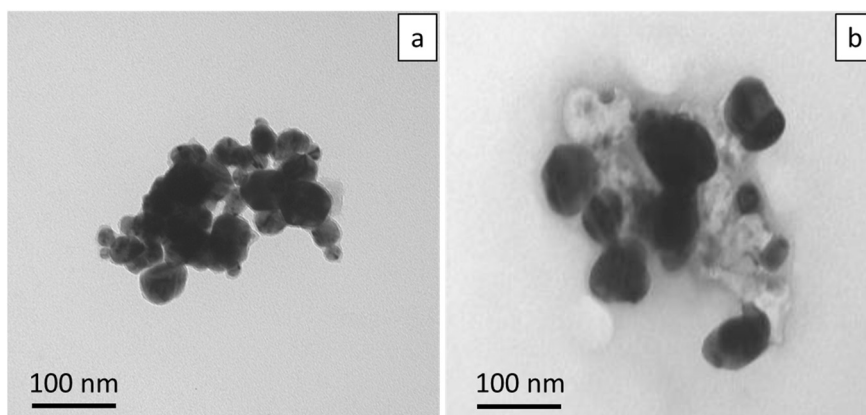

Fig. 1 TEM micrographs of a) a 30 nm AgNP agglomerate and b) an AgNP agglomerate.

fragmentation rates for the plastic materials, *e.g.*, plastics toys left degrading and fragmenting on the shore.[12–14] The experimental setup and the protocol are briefly summarized here. A rotationally stationary plastic sample is pressed down with weights onto an abradant plate attached to a variable speed motor shaft. A torque meter inserted between the abradant plate, and the motor is used to measure the rotational force applied during abrasion. The power input to the abrasion process can be expressed as a function of the angular velocity and the torque applied to the rotating abrading element and the normal force (weight) applied to the sample.

The abrasion process occurred in an enclosed space that allowed for abraded MPs to be collected for further analysis. Abrasion rates for different normal forces were obtained by varying the weight from 0.1 kg to 2 kg. Torque on the abrader was measured and this allowed the characterization of the friction coefficient for the abrading surface and the
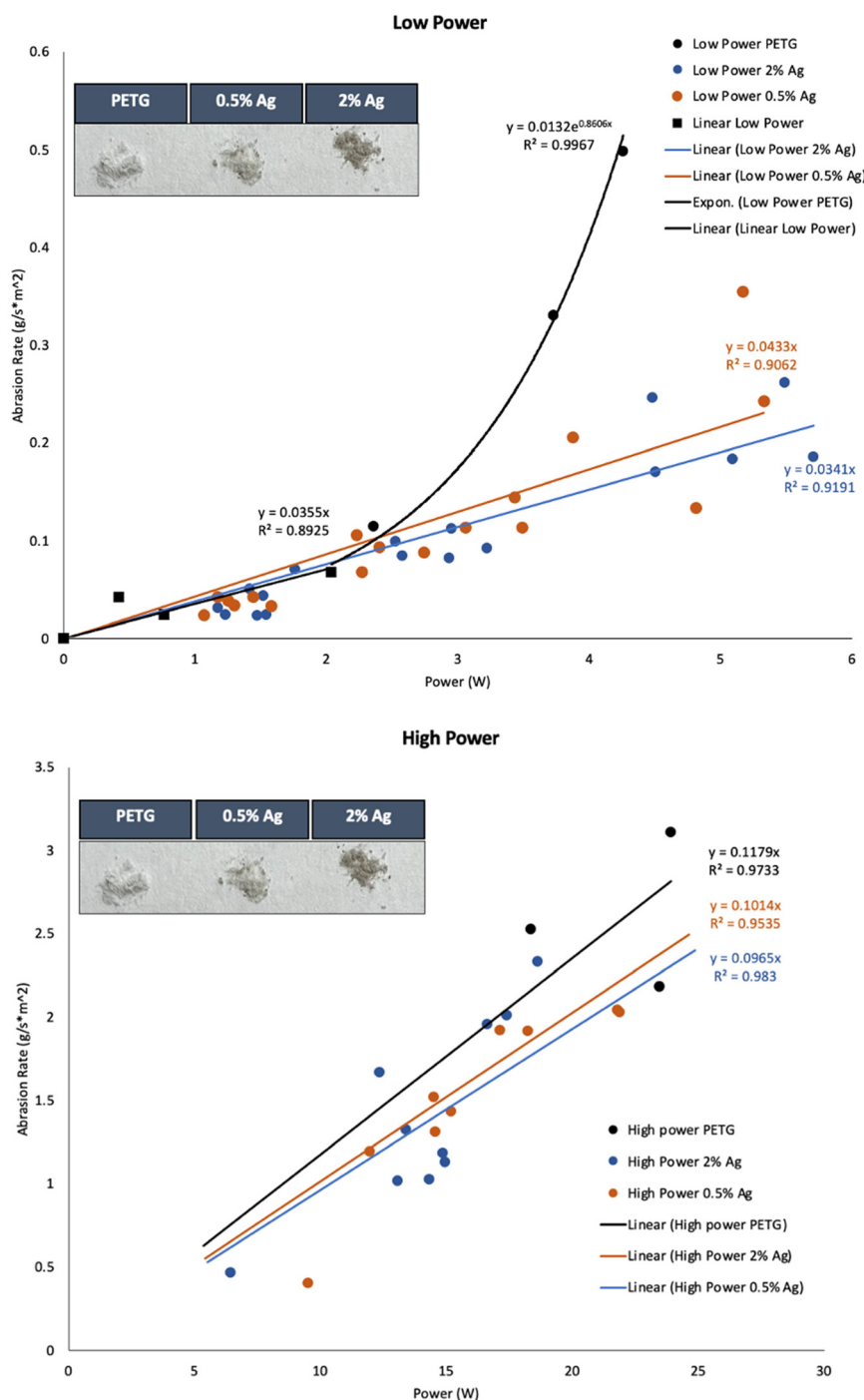

Fig. 2 Abrasion rate *versus* power of PETG, 0.5%Ag and 2%Ag obtain with P100 sandpaper. top) Low power bottom) High power.

2970 | *Environ. Sci.: Nano*, 2024, **11**, 2968–2977

This journal is © The Royal Society of Chemistry 2024

associated power inputs. Abrasion rates at a given power input were calculated by weighing samples before and after one minute of abrasion while maintaining a rotational speed between 13.3 Hz (800 RPM) and 16.7 Hz (1000 RPM). A 100-grit gold-colored aluminum oxide sandpaper (P100) was used as the abradant. After cleaning the inside of the chamber with cleanroom wipes, a hosed fume extractor was placed over the machine. The sandpaper was changed after every abrasion run to ensure it was not excessively worn. Abrasion rates were measured over a range of power input from 0 W to 200 W, and a power input $vs.$ abrasion rate plot (Fig. 2) was generated for each of the three composites (varying by Ag NP content) used in this study.

2.4 Abraded particle characterization

Abraded particles were collected from the bottom of the abrasion chamber on translucent drafting paper liner. The size distribution of particles was measured using a Mastersizer 3000 (Malvern, UK) laser diffractometer in batch modes (1 g L^{-1}). Since polymer particles strongly agglomerate in water, the particles were dispersed in 95% purified ethanol (Fischer Scientific). Particle morphology was determined by depositing the particles onto a double-sided copper tape and imaging with a scanning electron microscope (SEM) (Thermo Fisher Scientific Apreo). Energy dispersive X-ray spectrometry was performed using an X-Max-N 150 silicon drift detector (Oxford Instruments, UK). Particle chemistry was assessed using Fourier transform infrared (FTIR) spectrometer (Thermo Scientific Nicolet 8700) (Fig. S11–S13†). Zeta potentials were taken by measuring electrophoretic mobility (EPM) using the Nanosizer NanoZS (Malvern Panalytical Ltd.) with particles dispersed in nanopure, moderately-hard freshwater, and ocean water (compositions detailed in ESI†). The remaining abrasion products were suspended in water to facilitate aquatic toxicity testing in a companion study by Chernick $et\ al.$ (is submitted to same journal as this paper).

2.5 Statistical analysis

The statistical analyses were performed using Excel with a p-value < 0.05 and a standard deviation on the average linear fits (see Table S1 in the ESI†). The data sets were run through linear model fits and summaries using R.[17] These statistical tests (residual plots, normal QQ, Cook's test, and scale location) are shown in the ESI† Fig. S2–S4 for each of the materials.

3 Results and discussion

3.1 Influence of AgNP on PETG mechanical properties

The results of the tensile strength tests ($N = 3$) on the AgNP PETG composites (Table 1) did not show statistically significant differences in the AgNP material properties. In contrast, AgNPs embedded in a polymer matrix have been shown by others to slightly increase ultimate tensile strength (UTS) and elastic modulus (YM) in biopolymers.[18]

Table 1 Mechanical properties of three PETG–AgNP composites. Uncertainties represent ±1 standard deviations

Sample name	Ultimate tensile strength (MPa)	Young's modulus (MPa)	Breaking strain (mm mm^{-1})
PETG	32.16 ± 2.16	692 ± 129	0.058 ± 0.004
0.5%Ag	34.21 ± 1.08	722 ± 48	0.060 ± 0.002
2%Ag	27.91 ± 2.92	620 ± 37	0.058 ± 0.001

3.2 Abrasion rate quantification of PETG–AgNP composites

In Fig. 2, the abrasion rate (g m^{-2} s^{-1}) is plotted as a function of input power using the method described in Bossa $et\ al.$ where the PETG–MWCNT composites were studied.[12] ESI† Table S1 contains standard deviation values for the linear fits. Unlike the MWCNT composites, the statistical results suggest that separating power and high-power differences better reflect the breakdown trends. For the PETG, powers from 2–6 W were best shown to be exponential fit supported by the residual plot and trendline. However, for low power under 2 W the points were considered outliers using Cook's distance plot and thus another low power linear fit was used. AgNP composites both followed a linear trend for low-power fits supported by statistical tests. All three composites were not statistically significant from one another at low power from 0–2 W. However, from 3–6 W the AgNP composites differ from the PETG. This suggests that the AgNPs prevent some of the fragmentation release once the polymer transitions and as friction factors. This is due to some adjacent heat that the AgNP's absorb due to tribological breakdown at the surface and the transition from low to high power breakdown since this trend is not seen at low powers from 0–2 W or high powers from 6–20 W. At high-power, the linear trends show that the PETG matrix drives the abrasion process. Both AgNP composites and the PETG polymer had high-power linear fits that were not statistically significant from one another.

We used these results to obtain estimates of plastic abrasion rates in two scenarios: mechanical wear (sanding to simulate the environmental aging) and chewing of plastic products since AgNP polymers are used in baby toys and food packaging. Power inputs during mechanical sanding are estimated to range from 1 W to 300 W depending on sander used. Consider, therefore, the case of a low power sanding scenario where 2%Ag composite is sanded with a power input of 1 W. The abrasion rate for this scenario is estimated to be 0.0964 g m^{-2} s^{-1} as calculated from the slope of the 2%Ag fit in Fig. 2 (0.0964) multiplied by the power input (1 W).[19] In this manner, values of abrasion rate during sanding (input power range from 1 W to 300 W) were calculated to be (0.2198 ± 0.0867 to 219.0 ± 0.94) g h^{-1}, (0.2681 ± 0.1833 to 188.4 ± 0.38) g h^{-1}, and (0.2111 ± 0.1536 to 179.3 ± 0.91) g h^{-1} for PETG, 0.5%Ag, and 2%Ag samples respectively.[19,20] These were calculated by using the surface area of each puck (0.00172 m^2) and 3600 seconds to calculate the total exposure in g h^{-1} of the nanocomposite. Before the results of the calculations, note that there was not a statistical difference between the three materials tested and

Table 2 D10, D50, and D90 particle sizes. Uncertainties represent ±1 standard deviations

Sample name	D10 (µm)	D50 (µm)	D90 (µm)
PETG	161.3 ± 122.2	695.5 ± 230.8	1803.3 ± 425.1
0.5%Ag	8.3 ± 0.1	39.8 ± 0.2	72.8 ± 0.5
2%Ag	63.7 ± 3.3	143.8 ± 4.4	235.7 ± 12.8

standard deviations were carried throughout from the abrasion rate slopes. This method is a powerful tool for risk assessment and while the fragmentation process may be different the interpretation, the approximate abrasion rate in terms of power input is agnostic to the underlying mechanism. For the chewing scenario, an estimate of a 0.175 W was used for the power input, calculated assuming a mean molar force for babies of 2.5 N based on an average baby jaw length of 52.5 mm and an instantaneous chew time of 0.75 seconds.[21,22] These parameters lead to abrasion rates during chewing of (0.6411 ± 0.2528) mg min^{-1}, (0.7820 ± 0.5346) mg min^{-1}, and (0.6158 ± 0.4479) mg min^{-1} for PETG, 0.5%Ag and 2%Ag, respectively. Environmental exposures can also be estimated from power inputs as described in Sipe *et al.*[13] Using ocean wave estimations, the calculated abrasion release rates were estimated to be $(1.67 \times 10^{-11} \pm 6.58 \times 10^{-11})$ g per day, $(2.03 \times 10^{-10} \pm 1.39 \times 10^{-10})$ g per day, and $(1.60 \times 10^{-10} \pm 1.17 \times 10^{-10})$ g per day for PETG, 0.5%Ag and 2%Ag, respectively. River shore release rates were higher and estimated to be (0.24 ± 0.04) g per day (0.2 ± 0.14) g per day and (0.47 ± 0.12) g per day for PETG, 0.5%Ag and 2%Ag, respectively. The highest release rates were obtained for an ocean shoreline scenario, with values of (17 ± 1) g per day, (16×11) g per day, and (13 ± 9) g per day for PETG, 0.5%Ag and 2%Ag, respectively. Details of these calculations can be found in the ESI† Table S2 through S6.
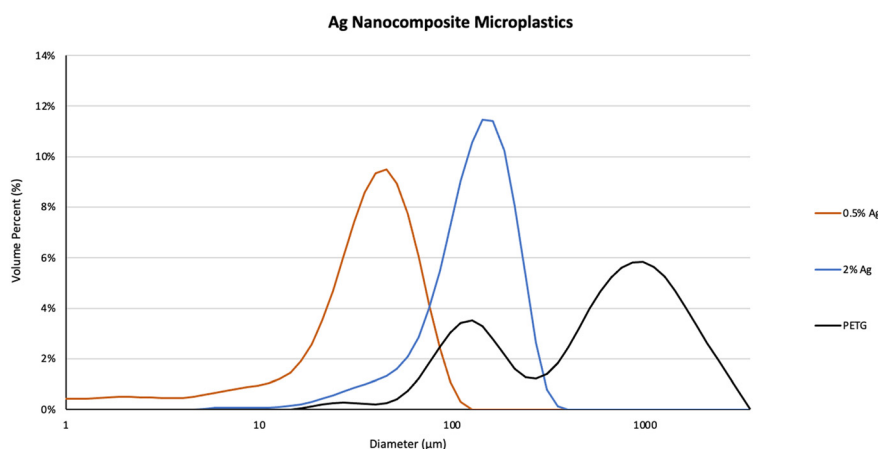
3.3 Abraded particles characteristics

The characteristics of abraded particles from PETG, 0.5%Ag, and 2%Ag sample, abraded using similar power input, were

compared. Particles were produced under the following abrasion condition: motor speed: 13.3 Hz (800 rpm), weight applied: 2 kg, abrading materials: P100 sandpaper. Particles generated during abrasion were collected once they settled in the abrader chamber and were then characterized.[12]

The particle size distributions of the settled particles were measured using static light scattering (SLS) as described in Bossa *et al.*[13] The D10, D50 and D90 are the diameters at which 10%, 50%, and 90% of the cumulative particle volumes are composed of particles with a diameter less than the respective values shown in Table 2. The D50 of PETG, 0.5%Ag and the 2%Ag were 695.5 µm, 39.8 µm, and 143.8 µm, respectively and the uncertainties were obtained using standard deviation of the six measurements used to obtain the average up to one decimal point. The particle sizes ranged from sub-micrometers to a couple hundred micrometers for 0.5%Ag and 2%Ag (Fig. 3) and from sub-micrometers to a few mm for PETG without Ag NPs. The PETG volume percent distribution of sizes was the widest due to a few fibrous particles which ranged in length up to 3.5 mm and skewed the distribution. Particles with the higher percentage of AgNPs (*i.e.*, abraded particles from 2%Ag) had a slightly larger diameter of nanocomposite MPs than the 0.5%Ag which averaged particle sizes under 100 micrometers.

This could be that the addition of silver led to smaller particle size distributions once abraded. While the 0.5%Ag and 2%Ag composite abraded particle size distributions quantified by DLS exhibit only one peak centered around 45 nm and 150 nm, respectively, there are two peaks, one centered around 120 nm and a second broad peak centered around 1 mm, in the PETG particle size distribution. The average glass transition temperature for each composite (N = 3) was 76.45 ± 3.69 °C for PETG, 79.03 ± 1.21 °C for 0.5%Ag and 78.31 ± 0.68 °C for 2%Ag (DSC figures shown in ESI† S2–S4). In addition, incorporation of nanoparticles into polymer composites can increase brittleness, especially if poorly dispersed.[23] Large fibrous particles in PETG abraded particles

Fig. 3 Size distribution of abraded particles from PETG AgNP composites.

2972 | *Environ. Sci.: Nano*, 2024, **11**, 2968–2977

This journal is © The Royal Society of Chemistry 2024

could be caused by melting during the abrasion process. This is supported by studies using unfilled *versus* filled polyethylene terephthalate (PET) nanocomposites and their tribological and mechanical behavior.[24,25]

The size and shape range of the nanocomposite particles are shown using SEM images in Fig. 4a–d. The inconsistency in particle size, shape, and homoaggregation of the PETG MPs are shown in Fig. 4a. This supports the SLS data shown in Fig. 3 where the larger particles measured are due to larger fibrous particles and homoaggregated MPs. These larger particles and homoaggregation were not seen in the 0.5%Ag or 2%Ag nanocomposite images shown in Fig. 4b and c. Studies in the synthesis of Ag NPs with polymers show that in the creation of AgNP aggregates in nanocomposites.[26] In Damm *et al.*, the particles produced from AgNP nanocomposites were smaller than their polymer-only counterparts and the interaction of polyamide supporting that the addition of AgNPs in a polymer matrix increases dispersion.[26,27] The SEM photos in Fig. 4d) show the AgNPs in large agglomerates. Energy dispersive X-ray spectrometry (EDS) mapping at 20 keV beam energy confirmed

the presence of Ag on the composite particles produced from abrasion. Fig. 5 shows the image of 2%Ag composites particles with Ag X-ray map overlay showing the locations of large AgNP agglomerates. Ag and C maps are normalized to highlight Ag and C signals. Additional SEM EDS results and their SEM images are presented in the ESI† Fig. S5–S9. Fig. 5 shows that the Ag in the released composite particles is highly aggregated and not well dispersed. Although this is seen in the particles released and not the composite, this suggests that the Ag aggregation can reduce the biocidal activity that the composite product was intended for.[28–30] A more homogenous distribution of Ag could increase biocidal activity and product efficacy if degradation of the product occurs after the use-phase due to the increased surface area of MPs.

3.4 Properties of abraded material in aquatic media

Zeta potential reflects the surface charge of nanoparticles in solution and informs on nanoparticle characteristics such as the state of the nanoparticle surface, the long-term stability of
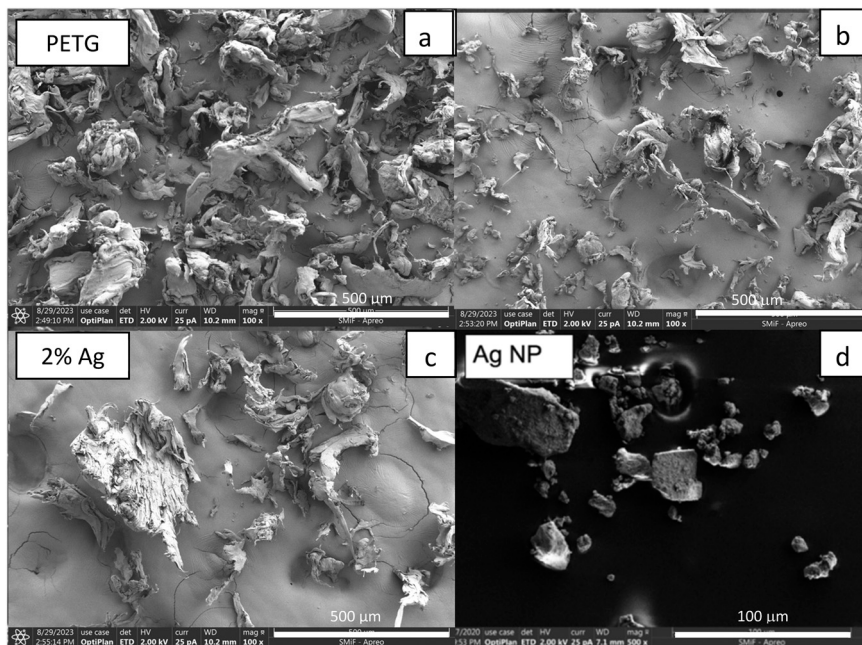

Fig. 4 SEM micrographs of a) PETG, b) 0.5%Ag, c) 2%Ag, and d) Ag nanoparticles. Note the scale bar ranges from 100 μm to 1 mm.
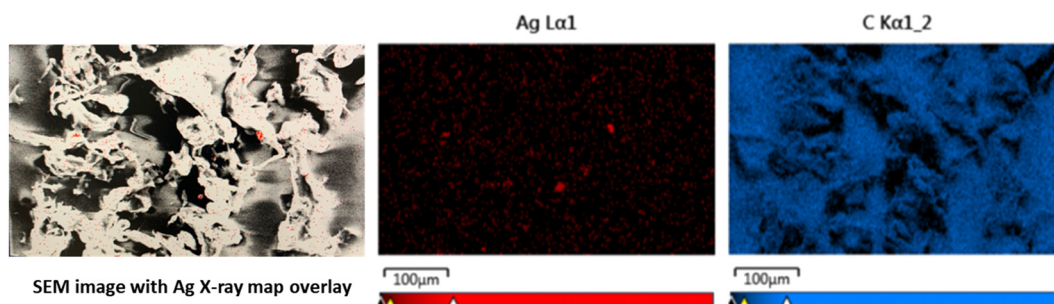

Fig. 5 SEM–EDS analysis of surface of 2%Ag abraded particles.

This journal is © The Royal Society of Chemistry 2024

Environ. Sci.: Nano, 2024, **11**, 2968–2977 | **2973**

a colloidal dispersion, and how a nanoparticle may interact with biological systems (*e.g.*, since most cellular membranes are negatively charged, cationic nanoparticles generally are more toxic and are associated with cell wall disruption).[31] Zeta potentials of abraded particles obtained from measurements of electrophoretic mobility in the three different aquatic media were very different (Fig. 6). In distilled water (pH: 6.8), AgNPs were negatively charged (-19 ± 3 mV) and abraded particles were also negatively charged with zeta potentials of -35 ± 11 mV, -31 ± 7 mV, and -5 ± 11 mV for PETG, 0.5%Ag, 2%Ag samples, respectively. As the AgNP content increased, the zeta potential values of the composites approached the charge of the pristine AgNPs. This increase was likely due to the increased presence of AgNPs at the surface of MPs (Fig. 6). The same trend was observed in freshwater (pH: 7.4) created from the standard methods for water and wastewater for moderately-hard freshwater.[32] In freshwater, zeta potentials were -20 ± 4 mV, -18 ± 6 mV, and -17 ± 7 mV for PETG, 0.5%Ag, 2%Ag samples, respectively, and -20 ± 6 mV for the AgNPs. In seawater (pH: 8.4) created with instant ocean, zeta potentials were -8 ± 2 mV, -8 ± 3 mV, and -11 ± 1 mV for PETG, 0.5%Ag, 2%Ag samples, respectively, and 4 ± 10 mV for the AgNPs. All the Zeta potential values, PETG, Ag composites, and AgNPs, were within the standard deviation of each other, indicating that the presence of AgNPs in the polymer (free or at the surface) has no difference to its behavior in freshwater. High ionic strengths such as those in of the seawater solution tend to mask the effects of the surface charge.[12] As with other colloids, a higher surface charge (or surface potential) may indicate a lower rate of particle–particle attachment in the case of MP aggregation as described in Jang *et al.* in which the link between removal efficiency and attachment was found to be highest at the isoelectric point.[33] Another reason for less aggregation with the Ag nanocomposites (shown in Fig. 4) and shown below in zeta potential could be the polarity distribution. PETG is nonpolar and has steric hindrance due to the large benzene and cyclohexane rings and the presence of Ag can help reduce that hindrance interaction with water.[34]

The hydrophilicity/hydrophobicity of the composite samples prior to abrasion was assessed by contact angle measured on a drop of deionized (DI) water (10 μL). The water contact angles were found to be $72° \pm 4.4°$, $80° \pm 5.5°$ and $110° \pm 5.9°$ for PETG, 0.5%Ag and 2%Ag, respectively, with the lower contact angles corresponding to a more hydrophobic surface. The addition of AgNPs created a more hydrophobic composite. As presented in ESI† Fig. S10, the shift of hydrophobicity is correlated with the Ag amount bulk. As contact is a surface measurement, we can express the amount of silver present at the surface is directly correlated with the bulk concentration. Ag in the nanocomposite is shown to alter the PETG characteristics at the surface of the composite and MPs and thus can change their behavior in environmental conditions and release. Pure Ag surface was tested in Bartell *et al.*, and show the maximum advancing contact angle of water over the surface was $95 \pm 0.5°$.[35] For superhydrophobic Ag_2O surfaces the contact angle for water can change from $0°$ to a hydrophobic $142°$ by adding additives such as pyridine.[36] For Ag_2S thin films, the addition of Ag on thin film composites cause a decrease of contact angle from $73.5°$ to $43.3°$ depending on the concentration.[37] These three examples demonstrate that pure Ag has a higher contact angle than the pure PETG tested, and as shown with Ag_2S adding Ag usually reduces the contact angle but the presence of additives in a polymer can cause the Ag effect increase as seen with the Ag_2O study. The unexpected increase of hydrophobicity could also be due to not being able to measure the same spot on the uneven 3D printed surfaces and the porosity due to the print design and the inherent gaps in which two filament strands meet. Hydrophobicity and zeta potential of the surface may also be affected by increases in porosity and surface area due to dissolution of AgNPs over time. This is supported in literature studies where the polarity of PETG is reduced as AgNPs are introduced to the polymer and the nanocomposites interaction when exposed to water.[34,38]
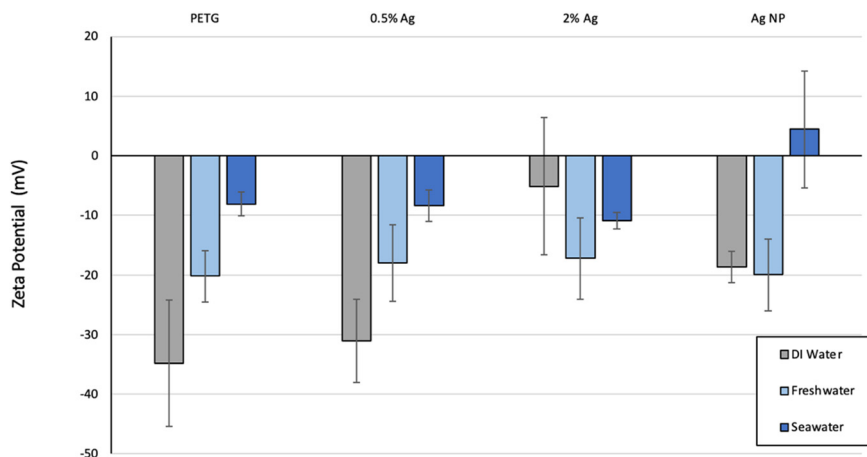

Fig. 6 Zeta potential (in mV) for the PETG, AgNP–PETG composites and AgNPs. Error bars represent ±1 standard deviations.

4 Conclusions

Addition of AgNPs as polymer filler, unlike other applications that seek to enhance mechanical properties, is to add antimicrobial functionality.[39] This study uses a novel abrasion apparatus and a NIST-CEINT (Center for the Environmental Implications of NanoTechnology) protocol to quantify abrasion of AgNP–PETG composites under various power inputs over time. These data can be used to estimate release of MPs from PETG and PETG composites used in a variety of consumer products. The data for both MWCNT composites, reported in a previous communication, and the AgNPs composites, investigated here, indicate that it is most likely the polymer matrix, rather than the nanofillers, that determine abrasion rate.[12] However, there are some changes with AgNP composites when studying low and high power abrasion fits. From 3–6 W it seems as though the AgNPs may help absorb the increase of fragmentation from the PETG polymer as the breakdown transitions from low to high power. While the PETG matrix in this study appeared to determine the abrasion behavior of the composites, the morphology of abrasion products differed based on the AgNP treatment, as did the surface chemistry of the abrasion products as characterized by electrophoretic mobility and contact angle data. The hydrophobicity of AgNP PETG composites can also be predicted with a linear relationship using the weight percent of AgNPs in the PETG composite.

Data availability

The data supporting this article have been included as part of the ESI.†

Conflicts of interest

There are no conflicts to declare.

Acknowledgements

References

1 M. Ahamed, M. S. Alsalhi and M. K. Siddiqui, Silver nanoparticle applications and human health, *Clin. Chim. Acta*, 2010, **411**(23–24), 1841–1848.

2 J. García-Barrasa, J. López-de-Luzuriaga and M. Monge, Silver nanoparticles: synthesis through chemical methods in solution and biomedical applications, *Open Chem.*, 2011, **9**(1), 7–19.

3 M. S. Blevens, H. F. Pastrana, H. C. Mazzotta and C. S.-J. Tsai, Cloth Face Masks Containing Silver: Evaluating the Status, *ACS Chem. Health Saf.*, 2021, **28**, 171–182.

4 T. M. Benn and P. Westerhoff, Nanoparticle silver released into water from commercially available sock fabrics, *Environ. Sci. Technol.*, 2008, **42**(11), 4133–4139.

5 S. Prasath and K. Palaniappan, Is using nanosilver mattresses/pillows safe? A review of potential health implications of silver nanoparticles on human health, *Environ. Geochem. Health*, 2019, 1–19.

6 A. Martínez-Abad, Silver- and Nanosilver-Based Plastic Technologies, in *Antimicrobial Polymers*, 2011, pp. 287–316.

7 T. Campbell, C. Williams, O. Ivanova and B. Garrett, Could 3D printing change the world, *Technologies, Potential, and Implications of Additive Manufacturing*, Atlantic Council, Washington, DC, 2011, p. 3.

8 M. E. Quadros, R. Pierson, N. S. Tulve, R. Willis, K. Rogers, T. A. Thomas and L. C. Marr, Release of Silver from Nanotechnology-Based Consumer Products for Children, *Environ. Sci. Technol.*, 2013, **47**(15), 8894–8901.

9 C. Rajbux, J. Pereira, M. D. C. Selbourne, A. R. Costa-Pinto and F. Poças, Assessment of baby Bibs. GC-MS screening, migration into saliva and insight of toxicity with QSAR tools, *Food Control*, 2020, **109**, 106951.

10 K. Song, R. Ding, C. Sun, L. Yao and W. Zhang, Microparticles and microplastics released from daily use of plastic feeding and water bottles and plastic injectors: potential risks to infants and children in China, *Environ. Sci. Pollut. Res.*, 2021, **28**, 59813–59820.

11 J. Zhang, L. Wang, L. Trasande and K. Kannan, Occurrence of Polyethylene Terephthalate and Polycarbonate Microplastics in Infant and Adult Feces, *Environ. Sci. Technol. Lett.*, 2021, **8**, 989–994.

This journal is © The Royal Society of Chemistry 2024

Environ. Sci.: Nano, 2024, **11**, 2968–2977 | **2975**

12 N. Bossa, J. M. Sipe, W. Berger, K. Scott, A. Kennedy, T. Thomas, C. O. Hendren and M. R. Wiesner, Quantifying Mechanical Abrasion of MWCNT Nanocomposites Used in 3D Printing: Influence of CNT Content on Abrasion Products and Rate of Microplastic Production, *Environ. Sci. Technol.*, 2021, **55**(15), 10332–10342.

13 J. M. Sipe, N. Bossa, W. Berger, N. von Windheim, K. Gall and M. R. Wiesner, From bottle to microplastics: Can we estimate how our plastic products are breaking down?, *Sci. Total Environ.*, 2021, 152460.

14 K. Scott, M. Wiesner, J. Sipe and N. Bossa, Correlating mechanical abrasion with power input, *NIST Special Publication*, 2022, **1200**, 30.

15 A. J. Kennedy, M. A. Chappell, A. J. Bednar, A. C. Ryan, J. G. Laird, J. K. Stanley and J. A. Steevens, Impact of organic carbon on the stability and toxicity of fresh and stored silver nanoparticles, *Environ. Sci. Technol.*, 2012, **46**(19), 10772–10780.

16 M. J. B. Amorim, S. Lin, K. Schlich, J. M. Navas, A. Brunelli, N. Neubauer, K. Vilsmeier, A. L. Costa, A. Gondikas, T. Xia, L. Galbis, E. Badetti, A. Marcomini, D. Hristozov, F. V. Kammer, K. Hund-Rinke, J. J. Scott-Fordsmand, A. Nel and W. Wohlleben, Environmental Impacts by Fragments Released from Nanoenabled Products: A Multiassay, Multimaterial Exploration by the SUN Approach, *Environ. Sci. Technol.*, 2018, **52**(3), 1514–1524.

17 R. C. Team, *R: A Language and Environment for Statistical Computing*, R Foundation for Statistical Computing, 2021.

18 A. Rozilah, C. N. A. Jaafar, S. M. Sapuan, I. Zainol and R. A. Ilyas, The Effects of Silver Nanoparticles Compositions on the Mechanical, Physiochemical, Antibacterial, and Morphology Properties of Sugar Palm Starch Biocomposites for Antibacterial Coating, *Polymers*, 2020, **12**(11), 2605.

19 M. R. Loredana and B. L. Anne-Marie, Research on Power Consumption for Sanding Process with Abrasive Brushes to Solid Spruce and MDF Panels, *Procedia Eng.*, 2015, **100**, 1495–1504.

20 B. Luo, L. Li, H. Liu, M. Xu and F. Xing, Analysis of sanding parameters, sanding force, normal force, power consumption, and surface roughness in sanding wood-based panels, *BioResources*, 2014, **9**(4), 7494–7503.

21 Y. Tadesse, D. Hong and S. Priya, Twelve Degree of Freedom Baby Humanoid Head Using Shape Memory Alloy Actuators, *J. Mech. Robot.*, 2011, **3**(1), 011008.

22 J. A. M. Schipper, M. J. S. van Lieshout, S. Böhringer, B. L. Padwa, S. G. F. Robben, R. R. van Rijn, M. J. Koudstaal, M. H. Lequin and E. B. Wolvius, Modelling growth curves of the normal infant's mandible: 3D measurements using computed tomography, *Clin. Oral Investig.*, 2021, **25**(11), 6365–6375.

23 A. J. Kennedy, A. D. McQueen, M. L. Ballentine, L. R. May, B. M. Fernando, A. Das, K. L. Klaus, C. B. Williams and M. J. Bortner, Degradation of microcystin algal toxin by 3D printable polymer immobilized photocatalytic TiO2, *Chem. Eng. J.*, 2023, **455**, 140866.

24 A. Bansal, H. Yang, C. Li, B. C. Benicewicz, S. K. Kumar and L. S. Schadler, Controlling the thermomechanical properties of polymer nanocomposites by tailoring the polymer–particle interface, *J. Polym. Sci., Part B: Polym. Phys.*, 2006, **44**(20), 2944–2950.

25 L. S. Schadler, L. C. Brinson and W. G. Sawyer, Polymer nanocomposites: A small part of the story, *JOM*, 2007, **59**(3), 53–60.

26 Y.-J. Cheng, D. N. Zeiger, J. A. Howarter, X. Zhang, N. J. Lin, J. M. Antonucci and S. Lin-Gibson, In situ formation of silver nanoparticles in photocrosslinking polymers, *J. Biomed. Mater. Res., Part B*, 2011, **97**(1), 124–131.

27 C. Damm, H. Münstedt and A. Rösch, Long-term antimicrobial polyamide 6/silver-nanocomposites, *J. Mater. Sci.*, 2007, **42**(15), 6067–6073.

28 S. Agnihotri, S. Mukherji and S. Mukherji, Impact of background water quality on disinfection performance and silver release of immobilized silver nanoparticles: Modeling disinfection kinetics, bactericidal mechanism and aggregation behavior, *Chem. Eng. J.*, 2019, **372**, 684–696.

29 I. L. Gunsolus, M. P. S. Mousavi, K. Hussein, P. Bühlmann and C. L. Haynes, Effects of Humic and Fulvic Acids on Silver Nanoparticle Stability, Dissolution, and Toxicity, *Environ. Sci. Technol.*, 2015, **49**(13), 8078–8086.

30 G. Metreveli, A. Philippe and G. E. Schaumann, Disaggregation of silver nanoparticle homoaggregates in a river water matrix, *Sci. Total Environ.*, 2015, **535**, 35–44.

31 N. M. Schaeublin, L. K. Braydich-Stolle, A. M. Schrand, J. M. Miller, J. Hutchison, J. J. Schlager and S. M. Hussain, Surface charge of gold nanoparticles mediates mechanism of toxicity, *Nanoscale*, 2011, **3**(2), 410–420.

32 L. S. Clesceri, A. D. Eaton, A. E. Greenberg, M. A. H. Franson, American Public Health Association, American Water Works Association and Water Environment Federation, *Standard Methods for the Examination of Water and Wastewater: 19th edition supplement*, American Public Health Association, Washington, DC, 19th edn, 1995.

33 M.-H. Jang, M.-S. Kim, M. Han and D.-H. Kwak, Experimental application of a zero-point charge based on pH as a simple indicator of microplastic particle aggregation, *Chemosphere*, 2022, **299**, 134388.

34 L. Y. Beeker, A. M. Pringle and J. M. Pearce, Open-source parametric 3-D printed slot die system for thin film semiconductor processing, *Addit. Manuf.*, 2018, **20**, 90–100.

35 F. Bartell and P. H. Cardwell, Reproducible Contact Angles on Reproducible Metal Surfaces. I. Contact Angles of Water against Silver and Gold1, *J. Am. Chem. Soc.*, 1942, **64**(3), 494–497.

36 W. Jiang, H. Fu, Y. Zhu, H. Yue, S. Yuan and B. Liang, Floatable superhydrophobic Ag2O photocatalyst without a modifier and its controllable wettability by particle size adjustment, *Nanoscale*, 2018, **10**(28), 13661–13672.

37 O. B. Nchoe, K. Matshetshe, M. As'ballim, P. Tetyana, K. Sikhwivhilu and N. Moloto, Fabrication of Ag2S-incorporated polyamide thin film nanocomposite reverse osmosis membranes with antifouling properties, *J. Appl. Polym. Sci.*, 2023, **140**(41), e54524.

38 C. J. van Oss, The interfacial tension/free energy of interaction between water and identical condensed-phase

2976 | *Environ. Sci.: Nano*, 2024, **11**, 2968–2977

This journal is © The Royal Society of Chemistry 2024

entities, i, immersed in water, w, in *Interface Science and Technology*, ed. C. J. van Oss, Elsevier, 2008, ch. 5, vol. 16, pp. 59–72.

39 K. Naik and M. Kowshik, The silver lining: towards the responsible and limited usage of silver, *J. Appl. Microbiol.*, 2017, **123**(5), 1068–1087.